J. Cent. South Univ. (2015) 22: 4372−4384
DOI: 10.1007/s11771-015-2986-8

Springer

Numerical investigation into effect of rear barrier pillar on stress distribution around a longwall face

JU Ming-he(鞠明和)[1, 2], LI Xue-hua(李学华)[1, 2], YAO Qiang-ling(姚强岭)[1, 2],
LI Dong-wei(李冬伟)[1, 2], CHONG Zhao-hui(种照辉)[1, 2], ZHOU Jian(周健)[1, 2]

1. School of Mines, China University of Mining and Technology, Xuzhou 221008, China;
2. Key Laboratory of Deep Coal Resource Mining of Ministry of Education (CUMT), Xuzhou 221008, China

Abstract: Numerical investigation was performed to examine the effect of rear barrier pillar on stress distribution around a longwall face. Salamon theoretical formula was used to calculate the parameters of the caving zone, which was later assigned to double yield constitutive model in FLAC^{3D}. Numerical results demonstrate that high stress concentration zone exists above the region where the second open-off cut intersects with the rear barrier pillar due to stress transfer and plastic zone expansion. It is also found that the maximum vertical stresses with varied distance to the seam floor are all within the projective plane of the rear barrier pillar and their positions concentrate on the barrier pillar adjacent to the connection corner of the second open-off cut. In addition, position of the maximum vertical stresses abruptly transfer from the connection corner adjacent to former panel to that adjacent to current panel along the panel direction.

Key words: numerical investigation; stress distribution; rear barrier pillar; second open-off cut; stress transfer

1 Introduction

Longwall mining, a preferred method when a high extraction ratio is required [1−2], is widely implemented by the Chinese coal industry with numerous modifications and improvements [3−4]. In longwall mining, the primary objective is to design coal pillars that are left in place to control mine stability and surface subsidence and, hence, to prevent damage to the surface or near-surface features, e.g., buildings, railways, highways, rivers, pipelines, etc [5]. Pillars, in general, are used in a mine to support the weight of overburden material between adjacent underground openings [6]. Therefore, it is important to design the optimal retaining width of the coal pillar and understand its effect on the adjacent roadways in longwall mining.

YANG et al [7] conducted numerical investigation into the reasonable width of a narrow coal pillar in gob-side entry driving, analyzed the difference in support conditions among roadway roof, entity coal side and narrow pillar side, and finally proposed the asymmetric control technique. WANG [8] built a mechanical model for strain softening pillar to analyze the progressive failure of pillar and proposed an instability criterion. SHABANIMASHCOOL and LI [9] employed two numerical models, a 3D local model and a 3D global model, to examine the stress changes in the barrier pillars during longwall mining and the influence of the longwall mining on the stress state in the border area in Svea Nord coal mine. CHEN et al [10] used the borehole pressure gauge to perform direct field monitoring to investigate the long-term bearing capacity of coal pillar. After an extensive reading of the literatures, we find that the published studies mainly focused on the design and stability of the narrow coal pillar in gob-side entry driving and the wide coal pillar in strip mining [11−12], with little attention being paid to the effect of a wide coal pillar in the rear of the coalface. Actually, this kind of rear pillar could form up either due to the constraints imposed by the geological setting or coal filed boundary or through changing the length of the panel to improve the recovery ratio [13]. Therefore, this pillar in the rear of the open-off cut, as illustrated in Fig. 1, is common in actual practice. However, the published papers concerning this kind of pillar are less. In view of this, we carried out the study to investigate the stress distribution characteristics around the open-off cut which is of great theoretical and realistic significance.

In this work, the intrusion of igneous rock results in a non-minable area in 8102 panel, which is divided into 8102A panel and 8102B panel, as shown in Fig. 2. Thus

Foundation item: Projects(51474208, 51304208) supported by the National Natural Science Foundation of China; Project supported by the Priority Academic Program Development of Jiangsu Higher Education Institutions (PAPD), China; Project(SKLCRSM12X01) supported by the State Key Laboratory of Coal Resources and Mine Safety, China University of Mining and Technology
Received date: 2014−10−20; **Accepted date:** 2015−02−10
Corresponding author: LI Xue-hua, Professor, PhD; Tel: +86−15950665233; E-mail: xuehua_cumt@163.com

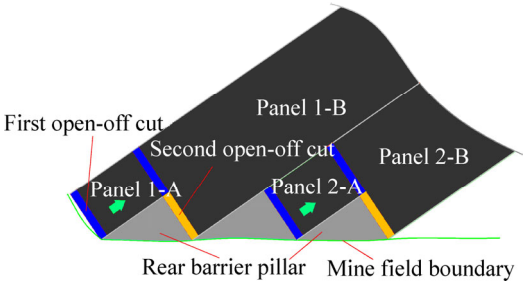

Fig. 1 Formation of rear barrier pillar

the non-minable area in the rear of 8102B panel forms the barrier pillar which is 70 m wide. We cannot help but asking which effect of this rear barrier pillar is on the stress distribution within front strata around a longwall face and how the stress distributes and changes in the strata above this 70-m-wide pillar during the extraction of panel. In order to address our concern, we carried out the numerical investigation to study the potential effect of barrier pillar subjected to igneous rock intrusion as well as the stress distribution and transfer characteristics in the strata above the 70-m-wide coal pillar.

2 Study site

This work is based on the 8102 coalface of Wolonghu coal mine in Huaibei city, Anhui Province, China. The longwall panel is located at a depth of approximately 520 m. The mined 8# coal seam has an average height of 4 m and an average dip angle of 5°. The detailed lay-out of the coalface is illustrated in Fig. 2. In Fig. 2, the 8101 panel was the first mining panel which has been mined out on February 15th, 2014 and the 8102 panel is the next panel whose extraction work commenced on March 5th, 2014. The gob-side entry retaining technology was adopted while mining the 8101 panel. Thus, the ventilation roadway of the 8101 panel can be maintained as the haulage roadway of the 8102 panel.

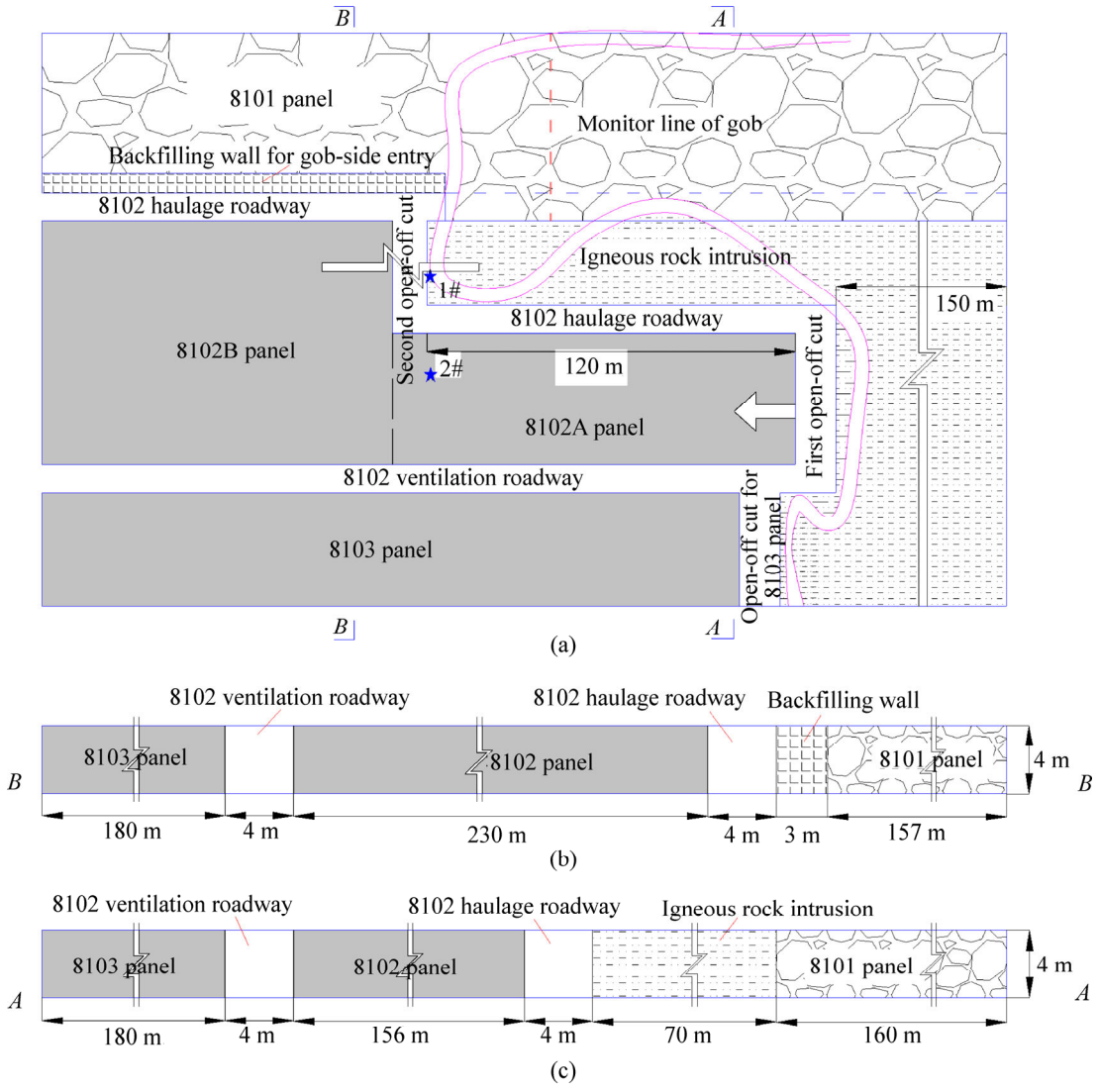

Fig. 2 Lay-out of panels in 8# coal seam and intrusion areas of igneous rock: (a) Floor plane of panels and roadways; (b) Sectional plane of $A-A$; (c) Sectional plane of $B-B$

Due to the intrusion of the igneous rock, as shown in Fig. 2, the metamorphic grade of the coal in some areas of the 8# coal seam increases. The intrusion of the igneous rock poses minor influence on the length of the 8101 panel and its extraction. However, it results in a non-minable area in 8102 panel, as shown in Fig. 2(c). The first open-off cut serves for the 8102A panel. After advancing 120 m, the coalface of the 8102A panel will arrive at the second open-off cut. Then, the width of the 8102A panel increases from 156 m to 226 m, forming the 8102B panel. As illustrated in Fig. 2, the 8102 panel is divided into two parts, 8102A panel and 8102B panel. Thus, the barrier pillar in the rear of the 8102B panel subject to the influences of the intruding igneous rock is left un-mined. This barrier pillar, to some extent, will have an impact on the stress distribution of the 8102B panel during its extraction which is worth our studying. Therefore, this work aims to investigate the possible effects of the rear barrier pillar on the stress distribution characteristics around the coalface.

According to the drilling log in the vicinity of the second open-off cut, we know that the immediate roof of the 8# coal seam is mudstone with an average thickness of 2.5 m, the main roof is siltstone with an average thickness of 6.0 m, and the immediate floor is mudstone with a thickness of 15.2 m. After conducting laboratory tests on the specimens, and considering the parameter conversion method proposed by the predecessors [14], we obtained the physical and mechanical parameters of the rock mass, which are given in Tables 1 and 2.

3 Numerical simulation of the caving zone

The finite element software, FLAC^{3D}, is adopted to establish the numerical model. The dimensions of the model are 300 m×270 m×80 m (length × width × height). The four sides of the model and its bottom are under displacement constraint. The vertical stress of 12.5 MPa is exerted on the top surface of the model. Mohr-Coulomb constitutive model is used to simulate the rock mass.

3.1 Theoretical calculation of the caving zone

After the extraction of the coal seam, the panel roof strata above the mined-out area or gob will be destressed.

Table 1 Physical and mechanical parameters of rock mass

Lithology	Thickness/m	Depth/m	Density/(kg·m^{-3})	Bulk modulus/GPa	Shear modulus/GPa	Cohesion/MPa	Friction angle/(°)	Tensile strength/MPa
Mudstone	35	462.7	2500	6.48	4.27	3.8	40	3.4
6# coal seam	1	497.7	1400	4.94	3.25	1.6	30	1.2
Mudstone	1.8	498.7	2480	8.33	4.3	3.7	40	3.2
Fine sandstone	1.2	500.5	2540	12.67	7.6	4.8	44	4.7
Siltstone	4.5	501.7	2520	11.54	7.26	4.5	43	4.5
Mudstone	2.0	506.2	2500	9.17	4.23	3.9	40	3.4
7# coal seam	1.5	508.2	1400	4.67	2.8	1.5	30	1.2
Mudstone	1.8	509.7	2480	6.67	4	3.8	40	3.5
Siltstone	6	511.5	2540	12	7.2	4.3	43	4.1
Mudstone	2.5	517.5	2480	9.47	4.88	3.8	40	3.4
8# coal seam	4	520	1400	4.76	3.28	1.6	30	1.2
Igneous rock intruding seam	4	520	2000	7	4.2	3.5	38	2.8
Mudstone	15.2	524	2500	7.5	3.46	4	42	3.4
Aluminum mudstone	3.5	539.2	2550	10.87	5.91	4.2	42	3.2

Table 2 Simulation parameters for caving zone

Strain	0	0.01	0.02	0.03	0.04	0.05	0.06	0.07	0.08
Stress/MPa	0	0.87	1.68	2.55	3.90	4.91	6.54	8.51	10.52
Strain	0.09	0.1	0.11	0.12	0.13	0.14	0.15	0.16	0.17
Stress/MPa	13.01	16.32	21.66	25.92	36.51	38.59	65.66	117.98	130.29

Density/(kg·m^{-3})	Bulk/GPa	Shear/GPa	Friction/(°)	Dilation/(°)
1500	10.42	4.81	15	5

With continued face advance, the immediate roof will collapse and cave into the gob area, and the disturbed roof strata gradually extend upwards [15]. Three zones of disturbance may be identified above the gob, a caved zone, a fractured zone and a continuous deformation zone [16]. After the collapse of the panel roof strata, the caving rocks in the gob will be gradually compacted with the advance of the panel. The stress of the gob will gradually increase to the virgin stress with the progressive compaction of the caving rocks. In order to simulate the strain hardening process of the gob, the double yield constitutive model in the FLAC^{3D} is adopted [17]. Knowledge of the consolidation behavior of the cave-in material is limited owing to the inaccessibility of the gob [18]. However, the Salamon model is a theoretical model which is widely used in describing the strain hardening behavior of rocks [19−20].

$$\sigma=\frac{E_0\varepsilon_v}{1-\varepsilon_v/\varepsilon_v^{\mathrm{m}}} \tag{1}$$

where σ is the applied compressive stress to the loose rocks, while the cave-in rocks are rigidly confined laterally; E_0 is the initial tangential modulus of the cave-in rocks; ε_v is the volumetric strain; $\varepsilon_v^{\mathrm{m}}$ is the maximum volumetric strain and can be obtained from the following equation [21],

$$\varepsilon_v^{\mathrm{m}}=\frac{b_{\mathrm{f}}-1}{b_{\mathrm{f}}} \tag{2}$$

where b_{f} is the bulking factor, which is determined by the height of the caving zone and the mining height.

$$b_{\mathrm{f}}=\frac{h_{\mathrm{c}}+h_{\mathrm{m}}}{h_{\mathrm{c}}} \tag{3}$$

where h_{m} is the mining height; h_{c} is the height of the caving zone in the roof which is related to the mechanical properties of the rock, the in-situ stress, the mining height and immediate strata, and the type and nature of the strata; h_{c} can be obtained through the empirical formula, $h_{\mathrm{c}}=100h_{\mathrm{m}}/(c_1h_{\mathrm{m}})+c_2$, where the values of c_1 and c_2 are given in Table 3.

Tangential modulus E_0 which is related to bulking factor, can be calculated from the following empirical formula,

$$E_0=\frac{10.39\sigma_{\mathrm{c}}^{1.042}}{b_{\mathrm{f}}^{7.7}} \tag{4}$$

where σ_{c} is the compressive strength of the rock pieces.

Table 3 Coefficients for average height of caving zone [21]

Strata lithology	Compressive strength/MPa	Coefficient	
		c_1	c_2
Strong and hard	>40	2.1	16
Medium strong	20−40	4.7	19
Soft and weak	<20	6.2	32

The virginal stress of the 8# coal seam is 13.2 MPa and the mining height is 4 m. The immediate roof is mudstone and the main roof is siltstone, whose thicknesses are 2.5 m and 6.0 m, respectively. The average compressive strength of the roof strata is larger than 40 MPa. According to the above formulae, we calculate the height of the caving zone as 16.6 m. Thus, the bulking factor used in this work is 1.241; the maximum strain of the cave-in rocks tends to be 0.19; the tangential modulus of the cave-in rocks is 92.05 MPa. Finally, the applied pressure derived from Salamon model for the cave-in rocks is

$$\sigma=\frac{92.05\varepsilon_v}{1-\varepsilon_v/0.19} \tag{5}$$

3.2 Calibration of numerical parameters for caving zone

The parameters of the numerical model are calibrated against the theoretical results derived from Salamon model. The fitted results are illustrated in Fig. 3. Table 2 shows the calibrated simulation parameters for the caving zone. Figure 4 shows the simulation results of the 8101 gob after adopting the double yield constitutive model and the calibrated parameters. In Fig. 4, the stress at the edge of the gob is small, with the minimum one being only 0.34 MPa; however, the stress in the gob gradually increases with the increasing distance to the edge of the gob. When the distance to the edge of the gob is 90 m, the stress reaches 10.7 MPa, where the stress recovers 81.1% compared with the virginal stress (13.2 MPa). This result is consistent with the field monitoring and theoretical analysis derived by the predecessors [21]. It also indicates that the parameters chosen in this simulation are reasonable. And stress

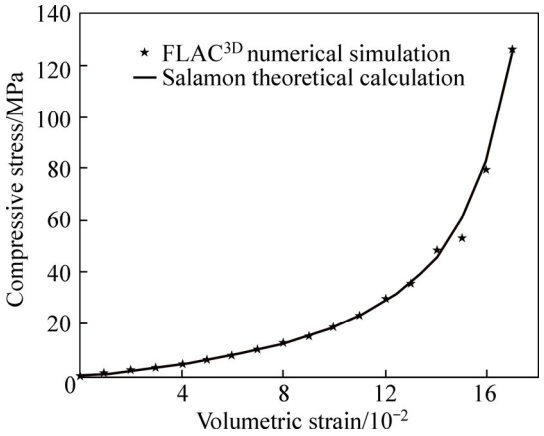

Fig. 3 Fitted curve of stress and strain of unit in caving zone

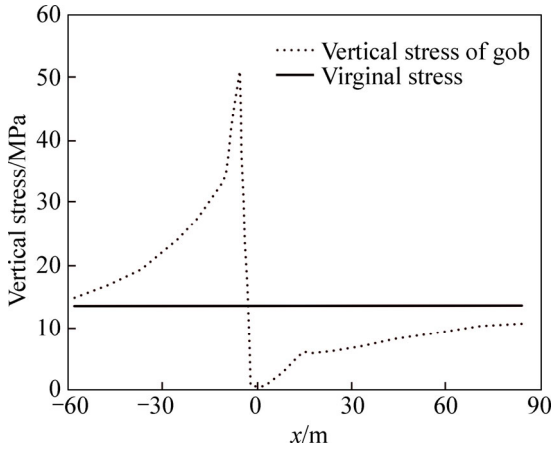

Fig. 4 Simulation curve of gob

concentration is observed in the corners of the gob. The maximum stress reaches 50.7 MPa with a concentration coefficient of 3.8. The vertical stress in the coal mass gradually decreases to its virginal level with the increasing distance to the edge of the gob.

4 Numerical simulation of longwall panel

Figure 5 shows the three-dimensional diagram of the numerical model. The intersection of the second open-off cut and the 8101 gob is the point *O*, set as the origin(x=0, y=0). According to the field monitoring results, the influencing distance of the advancing panel is about 60 m. Therefore, we analyze the effect of the advancing panel on the strata around the second open-off cut when the panel advances from −90 m to 90 m along the y-axis direction. This advancing distance is sufficient enough for us to investigate the effect of the un-mined 70-m-wide pillar (the rear barrier pillar) subject to igneous rock intrusion on the stress distribution characteristics around the longwall face. During the simulation of the advance of the panel, each excavation step is 3 m in the model. With one step lagging behind the excavation, the double yield constitutive model is employed to assign the parameters obtained in Section 3 (Table 2) to the rocks in the caving zone. The parameters

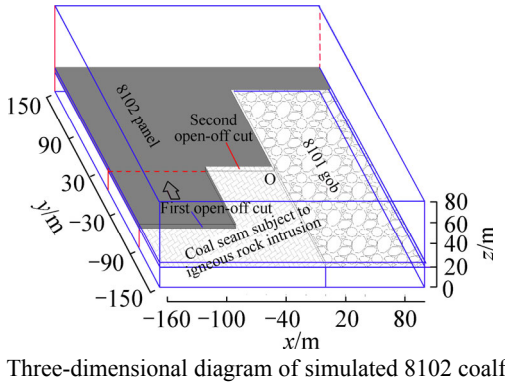

Fig. 5 Three-dimensional diagram of simulated 8102 coalface

for the other rocks remain unchanged, which are consistent with Table 1.

4.1 Stress distribution of strata around second open-off cut

Figures 6(a) to (d) illustrate the stress distribution of the strata around the second open-off cut when the coalface is 0 m, 30 m, 60 m and 90 m ahead of the second open-off cut, respectively. From Fig. 6(a), we know that the vertcial stress concentrates in the 70-m-wide pillar adjacent to the 8101 gob when the coalface advances at the second open-off cut and the stress concentration zone is within the #8 coal seam where the stress reaches 45.3 MPa with a stress concentration coefficient of 3.4 (45.3/13.2 MPa). When the 8102 coalface advances 30 m ahead of the second open-off cut, the maximum vertcial stress decreases from 45.3 MPa to 26.0 MPa, decreasing by 42.6%. In the mean time, the position of the stress concentration zone changes upwards from 1.5 m to 24.9 m away from the #8 coal seam floor. The simulation results with double yield model reveal that the height of the caving zone is 20.6 m away from the seam floor, which illustrates that the vertical stress concentration zone is above the critical upper boundary of the caving zone. From Figs. 7(a) to (b), we can know that the reason is the occurrence of the plastic zones around the 70-m-wide pillar. Because three sides of the pillar at the second open-off cut are exposed, the shallow roof rocks above the pillar suffer plastic failure and the stress transfers to the elastic zone resulting in the stress concentration zone above the pillar (Fig. 6(b)).

When the 8102 coalface advances 60 m ahead of the second open-off cut, the maximum stress concentration zone still hangs above the 70-m-wide pillar with a slight increase of its maximum value, rising from 26.0 MPa to 28.7 MPa, rising by 10.4%. However, the position of the zone decreases slightly from 24.9 m to 24.2 m away from the #8 coal seam floor, decreasing by 2.8%. With the gradual compaction of the caving zone around the second open-off cut, the bearing capacity of the above strata increases, resulting in a slight increase of the maximum vertical stress and a slight decrease of the stress position, as shown in Figs. 6(b) and (c). In the mean time, it is observed that the maximum stress above the pillar gradually transfers from 8101 gob side to the 8102 gob side.

Figures 6(c) and (d) show that when the 8102 coalface advances 90 m ahead of the second open-off cut, the maximum stress concentration zone transfers to the 8102 gob side with a further decrease of its position, being 22.8 m away from the #8 coal seam floor. In addition, the maximum stress value increases from 28.7 MPa to 33.4 MPa, increasing by 16.4%. The reason

is also due to the gradual compaction of the caving zone. From Fig. 6(d), we know that another stress concentration zone occurs above the 70-m-wide pillar with 42.5 m away from the #8 coal seam floor. The forming reason is the same as that for the first one, which is due to the plastic failure of the shallow roof rocks and the transfer of the stress to the elastic zone (illustrated by Fig. 7(d)).

Figure 8 shows the maximum vertical stress forming above the 70-m-wide pillar during the advance of the 8102 coalface. With the advance of the coalface, the vertical stress, concentrating in the vicinity of the two sides of the pillar, tends to be a saddle-shaped curve and the stress above the gob gradullay recovers to the original level. Figure 8(b) demonstrates that the stress in the secondly forming stress concentration zone above the pillar is smaller than that in the firstly forming one. However, due to the insufficient recovery of the stress in the gob and caving zone, the stress in the secondly forming stress concentration zone above the gob with 42.5 m away from the #8 coal seam floor is larger than that in the firstly forming stress one.

Figure 9 illustrtaes that the vertical stress above the 70-m-wide pillar has a sharp drop after the 8102 coalface

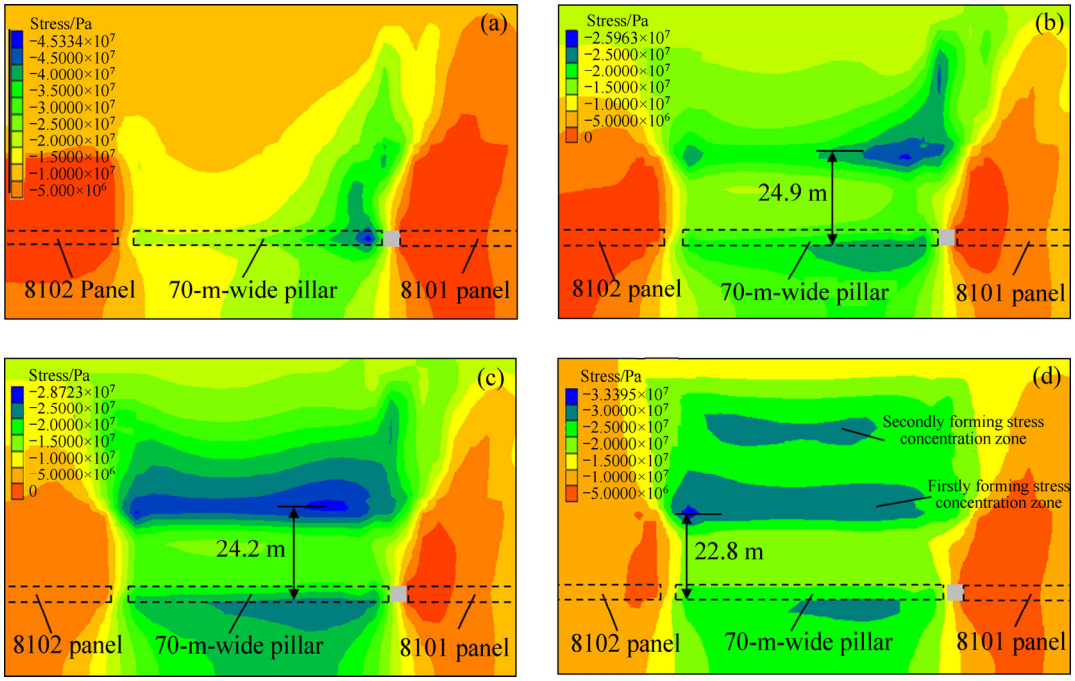

Fig. 6 Vertical stress distribution of strata around the second open-off cut with various distances between coalface and the second open-off cut: (a) 0 m; (b) 30 m; (c) 60 m; (d) 90 m

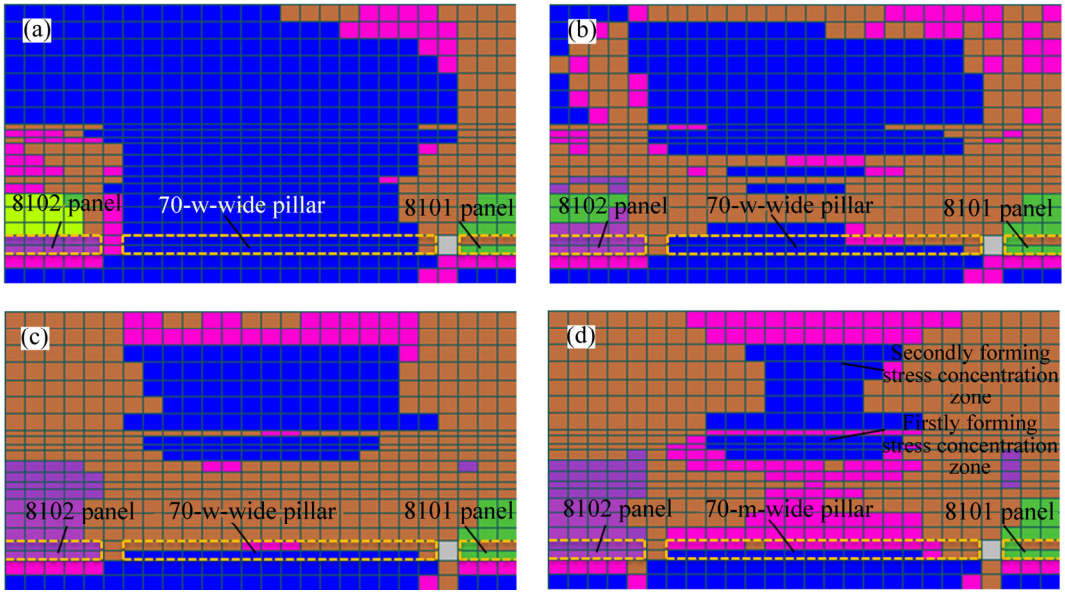

Fig. 7 Distribution of plastic zone within strata around the second open-off cut with various distances between coalface and the second open-off cut: (a) 0 m; (b) 30 m; (c) 60 m; (d) 90 m

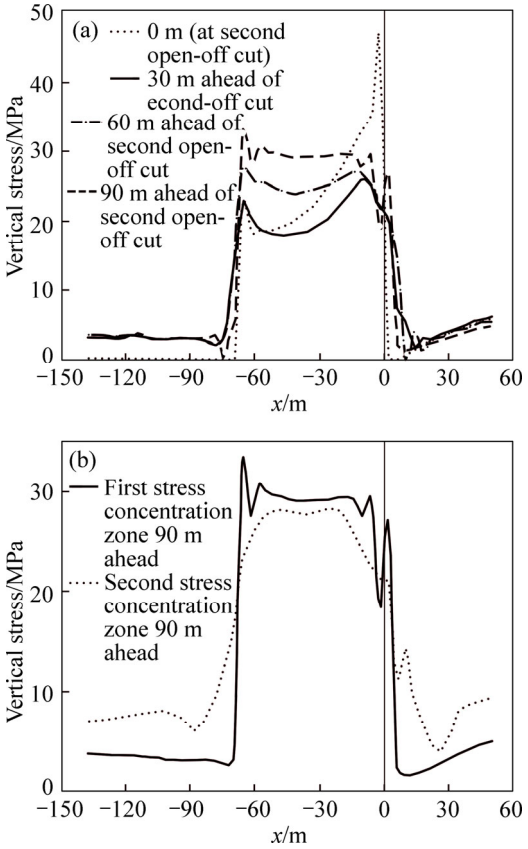

Fig. 8 Distribution of vertical stress in concentrate zone above the second open-off cut: (a) Comparison of vertical stress with various ahead distances of coalface to the second open-off cut; (b) Comparison of vertical stress between two concentrate zones when the ahead distance is 90 m

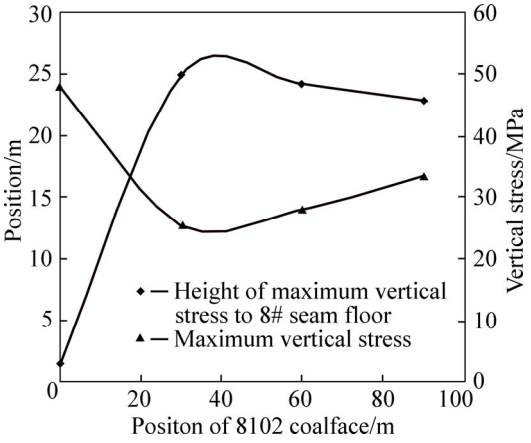

Fig. 9 Maximum value of vertical stress above pillar and its distance to #8 seam floor

reaches the second open-off cut, while the position of the maximum vertcial stress has a sharp rise. After the 8102 coalface passes the second open-off cut, the maximum stress and its position around the second open-off cut undergo small changes and with the continous advance of the coalface, they both gradually reach stability.

Figure 10 shows that when the 8102 coalface reaches the second open-off cut, the maximum vertical stress above the 8101 gob-side pillar is 58.9 MPa and the distribution of the stress above the second open-off cut manifests itself as a concave curve, which can also be verified by the data obtaining from the hydraulic shield support pressure real-time monitoring system (Fig. 11).

The support pressure in the verges of the 8102A coalface is higher than that in the middle of the second open-off cut, resulting from the superimposed effects of the front abutment pressure induced by the advance of the 8102 coalface and the side abutment pressure caused by the 70-m-wide pillar. The pressure reaches the maximum value at a 33 m distance to 8102 haulage roadway, which is close to 35.4 m (the field monitoring initial caving interval of the 8102 coalface). Therefore, we can see that the roof weighting characteristics are consistent with the "O-X Failure Pattern" [22], proving the reliability of the real time monitoring system. Thus, during the connection of the first open-off cut with the second open-off cut, support in the regions close to boundaries of the second open-off cut should be strengthened and the setting load of the hydraulic props shoud be strictly added according to the stipulation, avoiding the potential risks induced by the high stress.

When the 8102 coalface advances 30 m ahead of the second open-off cut, the stress within the strtata above the 8101 gob has approximately recovered to its virginal level. However, the stress within the strata above the 8101 gob is undergoing a severe recovering process, the high stress in the 8101 gob-side pillar experiences minor changes, while the stress in the 8102 gob-side pillar rises significantly. After that, with the continous advance of the coalface, the stress in the 70-m-wide pillar changes insignificantly as shown in Fig. 10(b).

The 1# and 2# shown in Fig. 2 represent the monitoring points, which record the stress changes in the 70-m-wide pillar and the stress changes in the 8102 coalface, respectively. The monitoring results are illustrated in Fig. 12. The results from 1# monitoring point show that the stress is in high state before the advancing of the 8102 coalface, which is 1.2 times higher than the vriginal stress (16.1/13.2 MPa). While, the 2# monitoring point is 120 m ahead of the 8102 first open-off cut, which is free from the impacts of the 8102 coalface.

The advance of the 8102 coalface starts to exert an influecne on the stress recorded by the 2# monitoring point when it is 60 m away from the 2# monitoring point. Figure 13 demonstrates the roadway surrounding rocks deformation before the connection of the first open-off cut with the second open-off. Taking the fact into account that the roadway will deform even without the influecnes of the advancing stress, we designate the 20 mm deformation as the lower limit for the influences of the advancing stress. Thus, the influential distance of

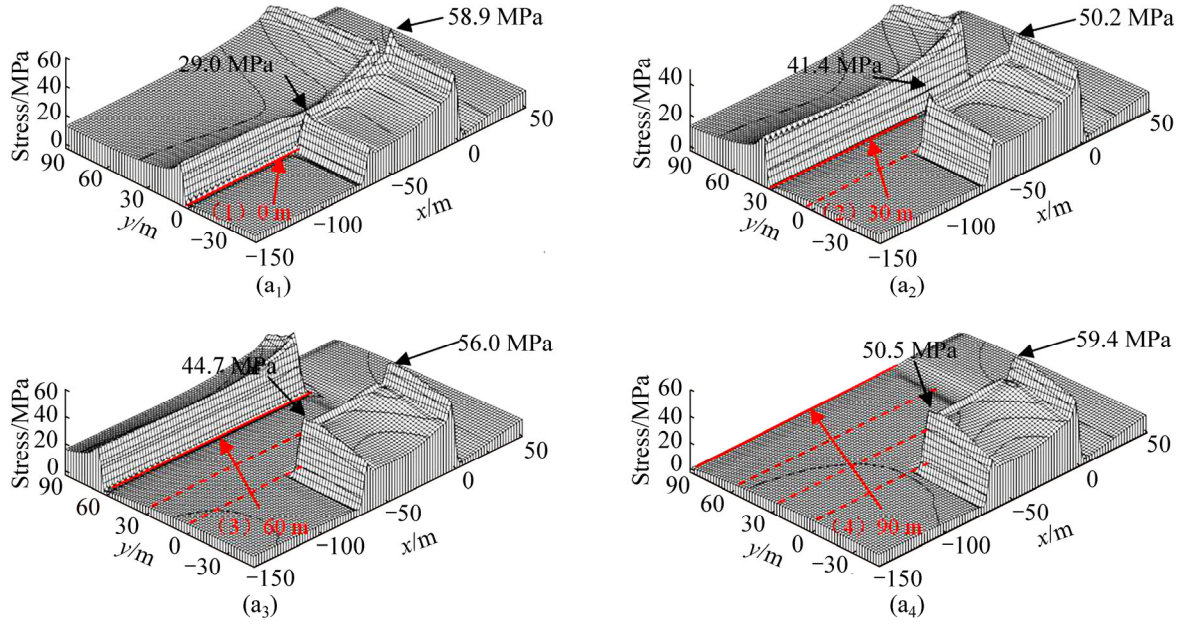

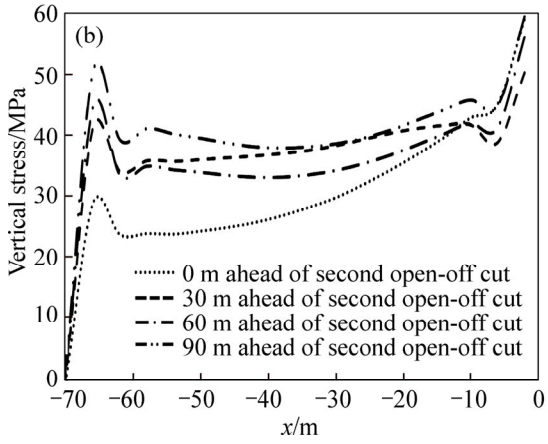

Fig. 10 Change of vertical stress of pillar and plane along advancing direction with various distances between the second open-off cut and 8102 coalface: (a_1) 0 m; (a_2) 30 m; (a_3) 60 m; (a_4) 90 m; (b) Vertical stress distribution of pillar adjacent to the second open-off cut

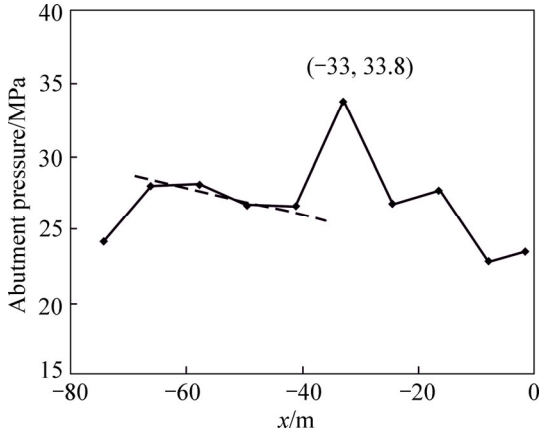

Fig. 11 Real-time monitoring data for hydraulic shield support pressure (It should be noted that real-time monitoring system is not installed in time. Data represent average value of working resistance of hydraulic shield support when coalface is 13.2 m to 22.8 m away along its advancing direction from second open-off cut)

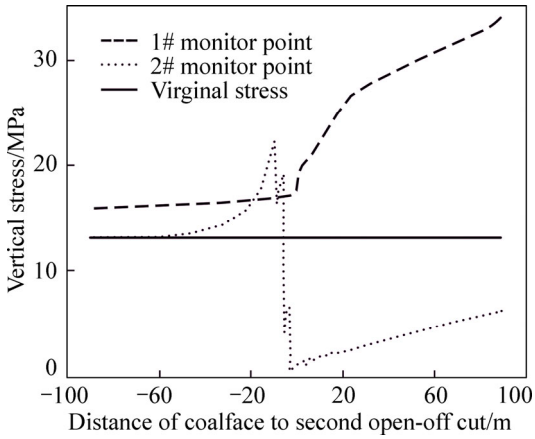

Fig. 12 Comparison between stress in 70-m-wide pillar and stress in 8102 coalface

the 8102 coalface advaning stress is about 60 m which is consistent with the simulation results of the FLAC^{3D} and the published research results [23−25]. When the coalface is 10 m away from the 2# monitoring point, the stress reaches the maximum value, 22.7 MPa, with a concentration coefficient of 1.7 (22.7/13.2MPa), which is also consistent with the field monitoring results.

After the 8102 coalface passes the 2# monitoring

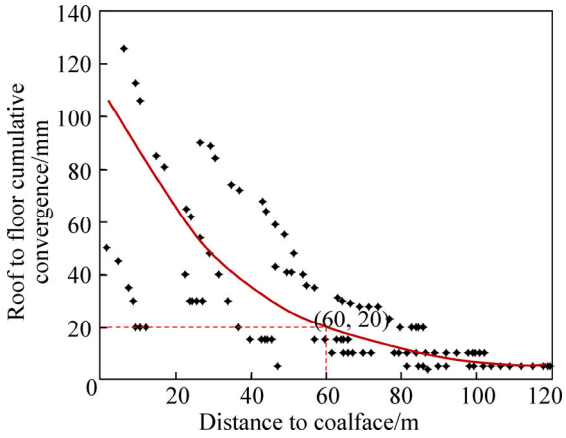

Fig. 13 Roof to floor cumulative convergence in haulage roadway before connection

point, the stress in the gob behind the monitoring point gradually recovers, while after the connection of the first open-off cut with the second open-off cut, due to the transfer of the stress above the gob to the back area of the wide pillar, the stress recorded by the 1# monitoring point gradually increases, changing from its previous stable state. When the 8102 advances 90 m ahead of the second open-off cut, the stress recored by the 1# monitoring point increases from 1.2 to 2.6 times larger than the original stress (34.1/13.2MPa).

4.2 Stress distribution characteristics of 70-m-wide coal pillar

The above research demonstrates that high stress concentration zones with certain height exist above the second open-off cut during the advance of the 8102 coalface of the 8102 coalface. LIANG et al [26] used FLAC to analyze the change of shear strain of overlying strata while mining, which can be combined to our research emphasis to investigate the interaction between them in order to reveal the mechanical characteristics of stress induced movement in specific position of strata. Besides, with the advance of the 8102 coalface, the stress gradually transfers from the 8101 gob side to the 8102 gob side. Therefore, we wonder whether the stress above or within the retained 70-m-wide coal pillar subject to igneous rock intrusion will have the similar stress distribution and transfer characteristics. For this purpose, we carry out further studies to investigate the stress distribution characteristics of the 70-m-wide pillar.

Figure 14(a) demonstrates that the position of the maximum vertical stress with a different distance to the bottom of the simulation model is characterized by regionalizing distribution in areas within the 70-m-wide pillar and adjacent to the second open-off cut due to the effects of the barrier pillar. Figure 14(b) shows that the distribution of the maximum vertical stress with a different distance to the bottom of the simulation model

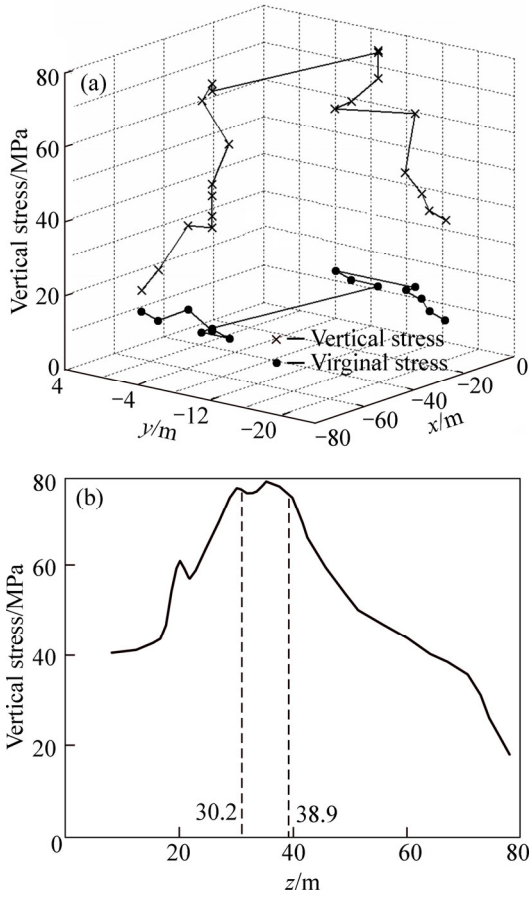

Fig. 14 Position of the maximum vertical stress with a different distance to bottom of simulation model (Floor of coal seam is 18.7 m to bottom of simulation model): (a) The maximum vertical stress and virginal stress in projection of pillar with various plane heights; (b) The maximum vertical stress projected to one plane with various heights to bottom of simulation mode

tends to be a parabolic curve. The stress stays at 76−79 MPa when the distance of the maximum vertical stress to the bottom of the simulation model is 30.2−38.9 m. Then, the maximum vertical stress gradually decreases to the original level with the increasing distance to the bottom of the simulation model. It can be concluded that the stress gradually tansfers towards the 70-m-wide pillar during the advance of the 8102 coalface, resulting in the overall stress rise within the pillar. The distribution of the position of the stress with different distance to the bottom of the simulation model is similar to the Section 4.1, which all reach the maximum at a certain distance to #8 coal seam roof, mainly resulting from expansion of the plastic zones within the overlying strata induced by the advance of the 8102 panel.

We unfold the distribution of the position of the maximum stress along the x−z plane and y−z plane of the 70-m-wide pillar to better analyze the stress distribution characteristics, which is shown in Fig. 15 and Fig. 16,

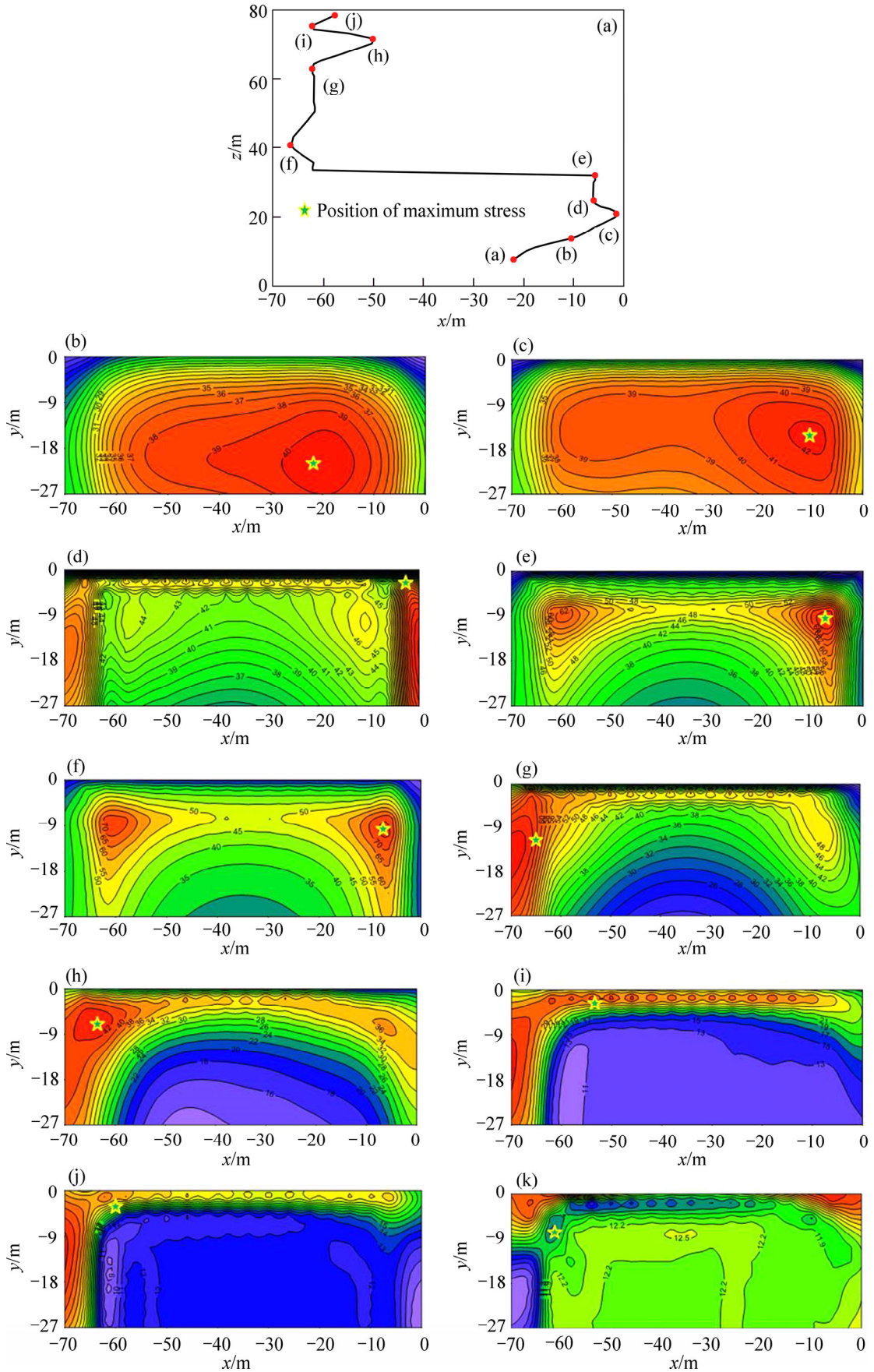

Fig. 15 Distribution of position of the maximum stress along x−z plane of 70-m-wide pillar: (a) Position of the maximum vertical stress of each plane height in projection of pillar; (b)−(k) Distributions of vertical stress projected in pillar for each plane height illustrated as Nos. (a)−(j) in (a)

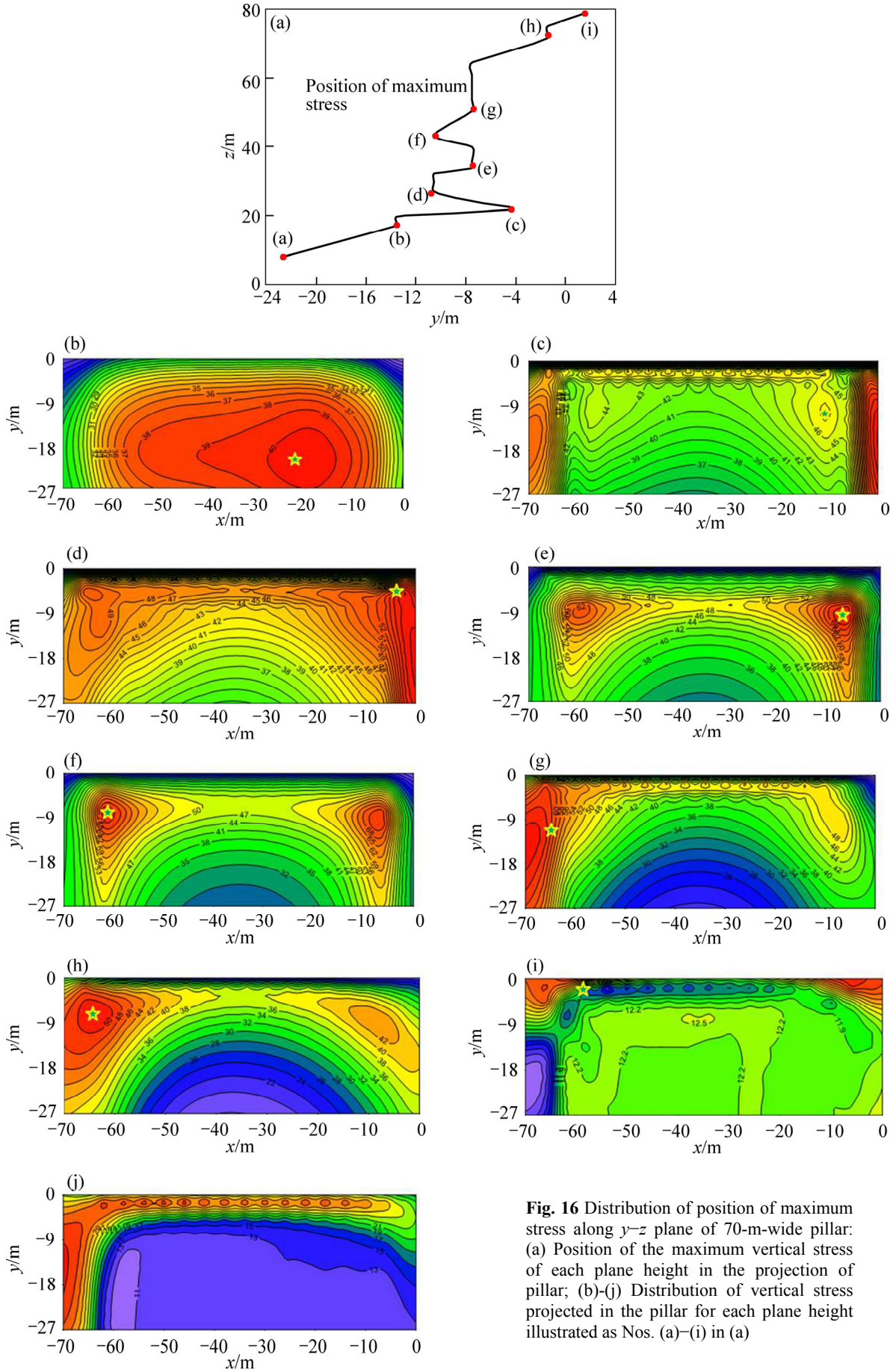

Fig. 16 Distribution of position of maximum stress along y−z plane of 70-m-wide pillar: (a) Position of the maximum vertical stress of each plane height in the projection of pillar; (b)-(j) Distribution of vertical stress projected in the pillar for each plane height illustrated as Nos. (a)−(i) in (a)

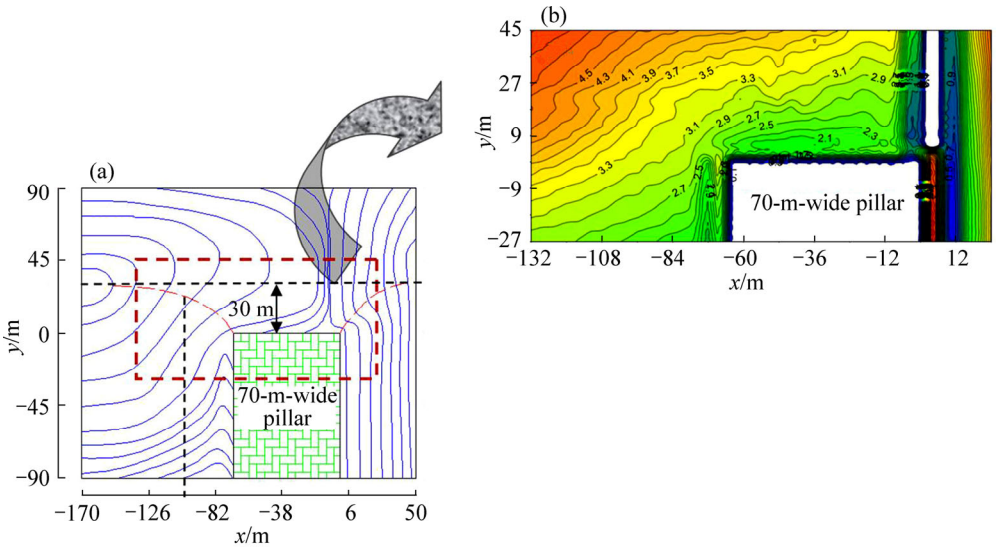

Fig. 17 Stress distribution around 70-m-wide pillar when 8102 coalface advances 90 m ahead of second open-off cut: (a) Profile of vertical stress distribution of gob around rear barrier pillar; (b) Specifically captured part of vertical stress distribution around pillar

respectively. Figure 15 shows that the maximum stress is close to the 8101 gob side when the distance of the stress to the bottom of the simulation model is 0−32 m. With the increase of the distance, the position of the maximum stress gradually transfers towards the 8102 gob. When the distance is z=27−40 m, the stress within the 70-m-wide pillar is symmetrically distributed in regard to the x direction and the stress is significantly higher than the stress with other distances. When the distance is larger than 32 m (13.3 m away from the 8# coal seam floor), the position of the maximum stress rapidly transfers towards the 8102 gob and maintains in the range of x from −65 to −50 m along the x axis. When the distance reaches z=78.2 m, the stress within the 70-m-wide pillar has already reached the virginal stress, indicating that the stress with this distance is free from the impacts of the barrier pillar. It should be noted that, in this work, the height of the model is 80 m, which may cause certain error. However, the general trend remains unchanged, and the influencing height of the 70-m-wide pillar is 55.5 m.

In Fig. 16, the position of the maximum vertical stress with different distances to the bottom of the simulation model is not only within the 70-m-wide pillar, but also adjacent to the second open-off cut. With the increasing distance of the strata to the bottom of the simulation model, the position of the maximum stress away 23 m gradually approaches the second open-off cut. Within the distance of z=20−68 m, the position of the maximum stress fluctuates, but, mainly concentrating on the range from −12 to −4 m along the y axis.

4.3 Stress distribution characteristics of gob around pillar

Figure 17(a) demonstrates that when the 8102 coalface advances 90 m ahead of the second open-off cut, 8102 gob does not compact in the typical form of "O-shape" [27]. The nearly arch-shaped distribution of the stress is found in the upper corner of the 70-m-wide pillar. However, 30 m distance away from the pillar, the caving and compaction of the 8102 gob is free from the impacts of the rear barrier pillar, forming the typical "O-shaped" compaction. It can be seen from Fig. 17(b) that stress around the 70-m-wide pillar adjacent to the 8102 gob side is small. With the increasing distance to the pillar, the stress gradually rises. The simulation results of the stress in the gob from the double yield model is consistent with the distribution characteristics, which proves the reliability of the adopted constitutive model.

5 Conclusions

1) This work uses the double yield constitutive model together with Salamon's empirical formula to deal with the rocks in the caving zone, which fully considers the stress changes in the gob and the overlying strata.

2) Stress distribution around the barrier pillar changes significantly when the coalface advances at a different distance to the second open-off cut. After the panel passing the second open-off cut, high stress concentration zone exists above the region where the second open-off cut intersects with the rear barrier pillar due to stress transfer and plastic zone expansion. With continuous advance of the panel, the maximum vertical stress within the high stress concentration zone gradually transfers from the side of former panel to that of current panel.

3) The maximum vertical stresses with varied

distance to the coal seam floor are all within the projective plane of the rear barrier pillar and their positions concentrate on the barrier pillar adjacent to the connection corner of the second open-off cut. With the increase of the distance, the positions abruptly transfer from the connection corner adjacent to former panel to that adjacent to current panel along the panel direction. In this study, the height of the abrupt position change is 13.3 m away from the coal seam floor and it gradually comes close to the second open-off cut along the advancing direction of the panel while 23 m away.

4) After panel extraction, the stress in the gob surrounding the rear barrier pillar distributes in the arc-shaped form along the corners of the pillar due to the existence of the 70-m-wide pillar. The influencing distance is about 30 m, where the mining height, coal seam depth and barrier pillar width are 4 m, 520 m and 70 m , respectively.

References

[1] BRADY B H G, BROWN E T. Rock mechanics: For underground mining [M]. New York: Springer, 2004.

[2] PENG S S. Longwall mining [M]. Morgantown, WV: West Virginia University, Department of Mining Engineering, 2006.

[3] GAO Fu-qiang, STEAD D, COGGAN J. Evaluation of coal longwall caving characteristics using an innovative UDEC Trigon approach [J]. Computers and Geotechnics, 2014, 55: 448−460.

[4] JU Jin-feng, XU Jia-lin. Structural characteristics of key strata and strata behaviour of a fully mechanized longwall face with 7.0 m height chocks [J]. International Journal of Rock Mechanics and Mining Sciences, 2013, 58: 46−54.

[5] WANG Hong-wei, JIANG Yao-dong, ZHAO Yi-xin, ZHU Jie, LIU Shuai. Numerical investigation of the dynamic mechanical state of a coal pillar during longwall mining panel extraction [J]. Rock Mechanics and Rock Engineering, 2013, 46(5): 1211−1221.

[6] WANG S Y, SLOAN S W, HUANG M L, TANG C A. Numerical study of failure mechanism of serial and parallel rock pillars [J]. Rock Mechanics and Rock Engineering, 2011, 44(2): 179−198.

[7] YANG Ji-ping, CAO Sheng-gen, LI Xue-hua. Failure laws of narrow pillar and asymmetric control technique of gob-side entry driving in island coal face [J]. International Journal of Mining Science and Technology, 2013, 23(2): 267−272.

[8] WANG Xue-bin. Analysis of progressive failure of pillar and instability criterion based on gradient-dependent plasticity [J]. Journal of Central South University of Technology, 2004, 11(4): 445−450.

[9] SHABANIMASHCOOL M, LI C C. A numerical study of stress changes in barrier pillars and a border area in a longwall coal mine [J]. International Journal of Coal Geology, 2013, 106: 39−47.

[10] CHEN Shao-jie, GUO Wei-jia, ZHOU Hui, SHEN Bao-tang, LIU Jiang-bo. Field investigation of long-term bearing capacity of strip coal pillars [J]. International Journal of Rock Mechanics and Mining Sciences, 2014, 70: 109−114.

[11] ZHANG Li-ya, DENG Ka-zhong, ZHU Chuan-guang, XING Zheng-quan. Analysis of stability of coal pillars with multi-coal seam strip mining [J]. Transactions of Nonferrous Metals Society of China, 2011, 21: s549−s555.

[12] ZHANG Yuan, WAN Zhi-jun, LI Fu-chen, ZHOU Chang-bing, ZHANG Bo, GUO Feng, ZHU Cheng-tan. Stability of coal pillar in gob-side entry driving under unstable overlying strata and its coupling support control technique [J]. International Journal of Mining Science and Technology, 2013, 23(2): 193−199.

[13] HOKE E, BROWN E T. Practical estimates of rock mass strength [J]. International Journal of Rock Mechanics and Mining Sciences, 1997, 34(8): 1165−1186.

[14] LU Cai-ping, DOU Lin-ming. The relationship between vertical stress gradient, seismic, and electromagnetic emission signals at Sanhejian coal mine, China [J]. International Journal of Rock Mechanics and Mining Sciences, 2014, 70(1): 90−100.

[15] GAO Fu-qiang, STEAD D, COGGAN J. Evaluation of coal longwall caving characteristics using an innovative UDEC Trigon approach [J]. Computers and Geotechnics, 2014, 55: 448−460.

[16] PENG S S. Coal mine ground control [M]. 2nd ed. New York: Wiley, 1986.

[17] ITASCA. FLAC3D version 4. 0 [M]. Minneapolis, Minnesota: Itasca Consulting Group Inc. 2009.

[18] WARDLE L. The use of numerical modeling for underground coal mine design [C]// HUDSON J A. Comprehensive Rock Engineering. Oxford: Pergamon, 1993: 733−748.

[19] PAPPAS D M, MARK C. Behavior of simulated longwall gob material [M]. US Department of the Interior, Bureau of Mines, 1993.

[20] SALAMON M D G. Mechanism of caving in longwall coal mining [C]// Rock Mechanics Contributions and Challenges: Proceedings of the 31st US Symposium. Golden, Colorado, 1990: 161−168.

[21] YAVUZ H. An estimation method for cover pressure re-establishment distance and pressure distribution in the goaf of longwall coal mines [J]. International Journal of Rock Mechanics and Mining Sciences, 2004, 41(2): 193−205.

[22] DOU Lin-ming, HE Hu. Study of OX-F-T spatial structure evolution of overlying strata in coal mines [J]. Chinese Journal of Rock Mechanics and Engineering, 2012, 31(3): 453−460. (in Chinese)

[23] XU Wen-quan, WANG En-yuan, SHEN Rong-xi, SONG Da-zhao, ZHANG Jing-min. Distribution pattern of front abutment pressure of fully-mechanized working face of soft coal isolated island [J]. International Journal of Mining Science and Technology, 2012, 22(2): 279−284.

[24] ZHANG Nong, ZHANG Nian-chao, HAN Chang-liang, QIAN De-yu. Borehole stress monitoring analysis on advanced abutment pressure induced by Longwall Mining [J]. Arabian Journal of Geosciences, 2014, 7(2): 457−463.

[25] WANG Hong-wei, JIANG Yao-dong, ZHU Jie, SHAN Ru-yue, WANG Chen. Numerical investigation on the assessment and mitigation of coal bump in an island longwall panel [J]. International Journal of Mining Science and Technology, 2013, 23(5): 625−630.

[26] LIANG S, ELSWORTH D, LI X, YANG D. Topographic influence on stability for gas wells penetrating longwall mining areas [J]. International Journal of Coal Geology, 2014, 132: 23−36.

[27] QIAN Ming-gao, XU Jia-lin. Study on the “O-shape” circle distribution characteristics of mining-induced fractures in the overlaying strata [J]. Journal of China Coal Society, 1998, 23(5): 466−469. (in Chinese)

(Edited by YANG Hua)